Relaxation kinetics of nano-ripples on Cu(001) surface

Wai Lun Chan, Ashwin Ramasubramaniam, Vivek B. Shenoy,* and Eric Chason
Division of Engineering, Brown University, Providence, Rhode Island 02912, USA
(Received 5 June 2004; revised manuscript received 7 September 2004; published 2 December 2004)

The relaxation of nano-ripples on Cu(001) is studied over a range of temperatures experimentally. Numerical simulations of relaxation of ripples are also carried out using a nonlinear continuum approach that accounts for the formation and interaction energies of surface steps and the Schwoebel barrier at the step edges. The total activation energy of the relaxation process is measured to be 1.18 ± 0.14 eV experimentally and 0.95 eV numerically. From these activation energies, it is clear that the system is in the regime where the relaxation kinetics is determined by attachment and detachment of atoms at step edges. Ripples are seen to decay with the formation of step-free regions or facets which indicates that the line tension of the steps plays an important role in the decay behavior. Although the ripples have a dominant spatial frequency or wavelength, our studies find that the decay behavior is not the same as that of a sinusoid of a single wavelength. The inherent nonlinearity of the evolution equations leads to significant coupling between the modes in the vicinity of the dominant wavelength. Numerical calculations that account for these coupling effects are in very good agreement with the experimental observations.

DOI: 10.1103/PhysRevB.70.245403 PACS number(s): 68.35.Fx, 68.47.De, 68.35.Md

I. INTRODUCTION

Mass transport on solid surfaces is a fundamental problem in materials science and has been the focus of experimental and theoretical interest over several decades. Material parameters that determine surface kinetics may be efficiently measured by studying the relaxation of surface features, such as sinusoidal ripples, which may be produced by lithographic techniques, ion sputtering or chemical etching. The relaxation behavior of amorphous surfaces and crystalline surfaces above the roughening temperature is well described by the continuum theory of Herring[1] and Mullins[2] and is well supported by the experimental work of Blakely and co-workers.[3,4]

The issue of surface evolution has found renewed interest over the past decade with the advance of nanoscale technology. The stability and evolution of nanostructures is strongly influenced by surface energetics owing to the small sizes of these structures. Typically, the growth and operating temperatures of these structures are much lower than the roughening temperature. Below the roughening temperature, a crystal surface close to a high-symmetry orientation has a stepped structure. The evolution of such a surface is controlled by the diffusion of atoms over the terraces as well as attachment and detachment of atoms at step edges and kink sites. The surface energy for such a stepped surface is determined by the energy required to form the steps as well as the energy associated with the entropic and elastic interactions of steps. A direct consequence of this is the presence of a cusp in the surface energy density at the high-symmetry orientation. The Herring-Mullins formalism cannot be trivially extended to this situation owing to the strong nonlinearities associated with the cusp. Previous modeling efforts have dealt with this problem by regularization methods,[5] free-boundary methods,[6] or by resorting to noncontinuum based models such as discrete-step[7,8] and Monte Carlo calculations.[9,10] Most of these studies have been restricted to the regime where the kinetics is determined by the diffusion of atoms along terraces (TDL kinetics)—those that do address the regime where attachment and detachment of atoms at step edges control the overall kinetics (ADL kinetics), do so in the absence of the line tension (i.e., the energy of formation) of steps. Recent experiments on two-dimensional ripples on Si(001)[11] and Ag(110)[12] as well as on sinusoidal gratings on Au(001) and Ni(001)[13] indicate, however, that the kinetics is likely to be in the ADL regime along with asignificant contribution from the step line tension.

More recent studies[14,15] have considered in detail the effect of step line tension and the influence of the kinetic regime on the relaxation of one-dimensional (1D) and two-dimensional (2D) sinusoidal modulations. These studies have shown that the decrease in the amplitude of the modulation can be described by simple power laws for various combinations of line tension and kinetic regime as

$$a(\tilde{t}) \sim \tilde{t}^{-1} \ (\beta_1 = 0),$$

$$a(\tilde{t}) \sim (\tilde{t}^* - \tilde{t}) \ (\beta_1 \neq 0), \ \text{(TDL kinetics)},$$

$$a(\tilde{t}) \sim e^{-\tilde{t}} \ (\beta_1 = 0),$$

$$a(\tilde{t}) \sim \sqrt{\tilde{t}^* - \tilde{t}} \ (\beta_1 \neq 0), \ \text{(ADL kinetics)}, \qquad (1)$$

where β_1 is the step line tension, $a(\tilde{t})$ is the amplitude of the modulation, $\tilde{t}$ is a nondimensional time whose exact form will be derived subsequently in this article and $\tilde{t}^*$ is the time at which the amplitude of the profile goes to zero. It is, however, not obvious that these power laws should hold for more general cases. In particular, roughness spectra for sputter rippled surfaces show the presence of several modes of comparable magnitude distributed around a peak value. Given the inherent nonlinearity of the surface evolution equations, mode-coupling effects could be significant thereby causing marked deviations from the behavior of single sinusoids. In the present work, we combine experi-

mental studies and numerical simulations to ascertain if there are indeed any such deviations from the above scalings and if mode-coupling effects are of significance. Nano-ripples are produced on Cu(001) using ion bombardment[16] and their relaxation behavior studied over a temperature range of 431–466 K using light scattering spectroscopy (LiSSp)[17] and atomic force microscopy (AFM). The evolution of the roughness spectrum with ripple decay allows us to extract information about both the scaling behavior of the individual modes in the roughness spectrum as well as the overall amplitude of the surface. We are also able to confirm the importance of the line-tension contribution from the presence of large step-free regions, or facets, seen in the AFM micrographs. To validate the theoretical framework for understanding the experimental observations, relaxation of actual sputter-rippled samples are numerically simulated with realistic parameters. While we find the results to be in good agreement both qualitatively and quantitatively, the behavior is found to be inconsistent with that of a single sinusoid owing to mode-coupling effects.

The organization of this article is as follows. In Sec. II, we describe the details of the sputtering process and the monitoring techniques. The theoretical framework for modeling the morphological equilibration of stepped crystalline surfaces is discussed in Sec. III. Section IV is devoted to the discussion and analysis of the experiments and the numerical simulations. The sputtered samples are annealed at different temperatures and the relaxation rate at each temperature determined. This information is used to obtain the temperature dependence of the relaxation rate which in turn allows us to estimate activation energies. It has been suggested in the past (e.g., Erlebacher *et al.*[11]) that the decay curves for individual modes can be collapsed onto each other by rescaling the relaxation time t as $\lambda^{-m}t$ where λ is the wavelength of the mode and the exponent m is determined by the kinetic regime. This would then allow for the use of data collapse as a means of determining the kinetics of the relaxation process. We examine this hypothesis both by experimental and numerical means and are led to conclude that such scaling behavior is unlikely owing to the inherent nonlinearity and mode coupling in the problem. Concluding remarks and further directions are provided in Sec. V.

II. EXPERIMENTAL DETAILS

Ripples with constant amplitude ($\sim$10 nm) and wavelength ($\sim$419 nm) are created on a Cu(001) surface by bombarding with 800 eV Ar+ ions at a glancing incidence inside a UHV chamber with base pressure of 2×10^{-9} Torr. The miscut of the sample surface is less than 1°. The orientation of the ripples is along the [110] direction. The sputtering process is carried out at 406 K. A description of the experimental details for ripple creation and characterization can be found in Chan, Pavenayotin, and Chason.[16] The temperature was monitored during sputtering and relaxation by a thermocouple embedded inside the heater; the embedded heater thermocouple was calibrated to another thermocouple on the sample surface not used during the actual experiments. Calibration runs indicate the rms deviation of the surface temperature during measurement is 1.0 K.

After sputtering to create ripples, the sample is heated to the annealing temperature (431–466 K) and the relaxation kinetics are measured from the point when the temperature of the sample becomes steady (these are referred to as the initial conditions for relaxation). The ripple amplitude during relaxation is monitored *in situ* by light scattering spectroscopy (LiSSp).[17] In this technique, the scattered intensity is proportional to the power spectral density (PSD) of the surface height. The spectroscopic approach allows for the measurement of the intensity of light scattered as a function of wavelength with fixed incidence and scatter angle. By using this technique, we are able to track in reciprocal space the intensity of different modes of the surface as a function of time for the same sample without having to pause the relaxation for measurement. The intensity of the light scattering measurements was calibrated relative to the ripple amplitude by *ex situ* atomic force microscope (AFM) measurements of the surface. Previous measurements have shown that the scattered intensity is proportional to the amplitude in the range measured.[17]

The light scattering measurements confirm that the amplitude of the initial surface was the same over different runs within a 10% uncertainty. This minimizes variations of the relaxation rate with initial amplitude and allows for comparison at different temperatures. Nevertheless, we consider the effect of the error of the ripple initial amplitude on the error in the relaxation rate, so that the error shown as the error bar in Fig. 4 includes the effect of the amplitude variation.

AFM was used to measure the morphology of samples removed at different stages of the relaxation process. This gives a series of real space images that show how the ripples decay. Care was taken to minimize any oxidation or contamination of the surface during removal. The AFM measurements were done within 15 min after the sample was unloaded from the vacuum chamber. Periodic measurements of the same surface showed that the surface morphology did not change significantly within a few hours after removal from the chamber.

III. THEORETICAL FRAMEWORK AND NUMERICAL METHOD

Prior to discussing the results of our experiments and pursuing further analyses, we outline briefly the continuum theory of morphological equilibration of a crystalline surface based on the underlying physics of surface steps. A detailed discussion may be found in Shenoy, Ramasubramaniam, and Freund,[14]—we offer only the relevant details here.

A. Continuum theory of surface evolution

Consider a free surface S with orientation dependent surface energy $\gamma(\nabla_S h)$ where h represents the height of the surface relative to a high-symmetry reference plane and $\nabla_S(\cdot)$ represents the surface-gradient operator. The free-energy F of this surface is given by

$$F = \int_S \gamma(\nabla_S h)\mathrm{d}S \tag{2}$$

and the rate of change of free-energy

$$\dot{F} = \int_S \mu v_n \mathrm{d}S \tag{3}$$

provides a definition for the surface chemical potential μ as the the driving force which is work conjugate to the change in surface shape owing to surface diffusion, v_n being the normal velocity of the surface. The mass flux $\mathbf{j}$ on the surface is a vector field related to the chemical potential through a kinetic relation of the form

$$\mathbf{j} = -M(\nabla_S h)\nabla_S \mu, \tag{4}$$

where $M(\nabla_S h)$ is a mobility parameter, in general a tensor field, that depends explicitly upon the local orientation, temperature and concentration of the diffusing species among other factors. We will assume the surface diffusion process to be isotropic for simplicity in the following discussion. Conservation of mass allows us to relate the change in surface shape to the surface diffusion process as

$$\frac{\partial h}{\partial t} \equiv v_n = -\nabla_S \cdot \mathbf{j}. \tag{5}$$

Equations (2)–(5) now provide a means of solution for the evolution of the surface shape and can be solved in their present form by standard numerical techniques as long as the chemical potential remains nonsingular. In the event of singularities appearing in the chemical potential, owing commonly to the presence of a cusp in the surface energy, the equations are no longer well behaved. It is, however, possible to reformulate and solve these in a variational form. To this end we define a functional

$$\Phi[\mathbf{j}^*] = \int_S \left[-\mu \nabla_S \cdot \mathbf{j}^* + \frac{1}{2}\frac{|\mathbf{j}^*|^2}{M(\nabla_S h)} \right] \mathrm{d}S, \tag{6}$$

which is readily obtained from Eq. (4) by the calculus of variations and an integration by parts under the assumption of periodic boundary conditions, $\mathbf{j}^*$ being any arbitrary flux that satisfies the same boundary conditions as $\mathbf{j}$. It may also be shown from the calculus of variations that the flux $\mathbf{j}^* = \mathbf{j}$, which satisfies Eq. (4) exactly, is a minimizer of the functional. We can thus develop a numerical scheme which seeks to determine an approximate solution $\mathbf{j}^*$, expressed using a suitable set of basis functions, that renders $\Phi[\mathbf{j}^*]$ a minimum.

It now remains to specify the exact form for the surface energy $\gamma(\nabla_S h)$ and the mobility parameter $M(\nabla_S h)$. The surface energy follows the usual description for stepped vicinal surfaces ($|\nabla h| \ll 1$) as

$$\gamma(\nabla h) = \gamma_0(T) + \frac{g_1(T)}{h_s}|\nabla h| + g_3(T)|\nabla h|^3, \tag{7}$$

where γ_0 is the surface energy density of the high-symmetry reference surface, $g_1(T)$ is the step-formation energy, $g_3(T)$ is the step-interaction energy and h_s is the step height. In general, $g_1(T)$ and $g_3(T)$ contain contributions both from energetic and entropic factors. For a high-symmetry step, a simple lattice model may be used to obtain these coefficients as[18]

$$g_1(T) = \frac{\epsilon_k}{a} - \frac{k_B T}{a}\log\left(\coth\left(\frac{\epsilon_k}{2k_B T}\right)\right),$$

$$g_3(T) = \frac{(\pi k_B T)^2}{24 h_s^3 \tilde{\beta}(T)}\left(1 + \sqrt{1 + \frac{4A\tilde{\beta}(T)}{(k_B T)^2}}\right)^2, \tag{8}$$

where $\tilde{\beta}(T)$ is the step stiffness, A is the strength of the dipolar elastic interactions between two steps, a is the near-neighbor spacing and ϵ_k is the kink formation energy, assumed for simplicity to be isotropic. The step stiffness for a high-symmetry step is in turn given by

$$\tilde{\beta}(T) = \frac{k_B T}{a}\sinh^2\left(\frac{\epsilon_k}{2k_B T}\right). \tag{9}$$

The surface energy density may now be rewritten as

$$\gamma(\nabla h) = \gamma_0(T) + \beta_1|\nabla h| + \frac{\beta_3}{3}|\nabla h|^3, \tag{10}$$

where $\beta_1 = g_1(T)/h_s$ and $\beta_3 = 3g_3(T)$. The mobility parameter is obtained by taking the continuum limit of the terrace mass flux equations obtained by the classic BCF approach[15] as

$$M(\nabla h, T) = \frac{\Omega^2 D_s(T) C_{eq}(T)}{k_B T}\frac{1}{1 + \dfrac{2D_s(T)|\nabla h|}{\kappa(T) h_s}}, \tag{11}$$

where Ω is the atomic volume, $D_s(T)$ is the adatom diffusion constant, $C_{eq}(T)$ is the equilibrium adatom concentration ahead of a noninteracting step and $\kappa(T)$ is the effective rate of attachment and detachment of adatoms at a step edge, the two rates usually being unequal owing to the Ehrlich-Schwoebel barrier.[19,20] The kinetics of mass transport is controlled by the length $\ell = D_s/\kappa$ which when compared to the typical terrace width Δx establishes the rate-limiting process. For $\ell \ll \Delta x$, the kinetics of mass transport is diffusion limited, whereas in the opposite limit, $\ell \gg \Delta x$, the kinetics is limited by attachment-detachment at step edges. For the former case, $D_s|\nabla h|/\kappa h_s \ll 1$, the mobility parameter is simply a constant $M(T) = \Omega^2 D_s(T) C_{eq}(T)/k_B T$ while in the latter case, $D_s|\nabla h|/\kappa h_s \gg 1$, the mobility parameter is inversely proportional to the local slope or, alternatively, the local step density as $M(\nabla h, T) = (\Omega^2 C_{eq}(T)\kappa(T) h_s/2k_B T)|\nabla h|^{-1}$. This recovers the result first derived by Noziéres[21] for attachment-detachment limited kinetics. Equation (11) allows for a continuous transition between these two limits.

B. Numerical method

We now proceed to outline a numerical method to solve the evolution equations derived above. Since sputter ripples are nearly one-dimensional features, the wavelength in one direction being significantly longer than the other, the details of the evolution process can be captured well by a (1D) model.[33] Furthermore, since surface slopes are relatively small, $\langle|\nabla h|\rangle = 0.05$ typically for the initial sample profile, we restrict attention to the small-slope limit. The height of the profile may be expanded in a complete set of periodic basis functions as

$$h(x,t) = \sum_{n=-N}^{N} a_n(t) \mathrm{e}^{inkx}, \tag{12}$$

where $k=2\pi/\lambda$ is the wave number and N is the number of modes used in the expansion. The mass flux can be written from Eq. (5) as

$$j(x,t) = -i \sum_{n=-N}^{N} \dot{a}_n(t) \frac{e^{inkx}}{nk}. \tag{13}$$

This can now be substituted into Eq. (6) to obtain

$$\Phi[\dot{a}_{-N}, \ldots, \dot{a}_N] = -\sum_{n=-N}^{N} ink\dot{a}_n(t) \int_0^\lambda \frac{\partial\gamma}{\partial h_x} e^{inkx} \mathrm{d}x - \frac{1}{2D} \times \sum_{m,n=-N}^{N} \frac{\dot{a}_m(t)\dot{a}_n(t)}{mnk^2} \int_0^\lambda \left(1 + \frac{|h_x|}{\epsilon}\right) e^{i(m+n)kx} \mathrm{d}x, \tag{14}$$

where $\epsilon=(2D_s/\kappa h_s)^{-1}$ and $D=\Omega^2 D_s(T) C_{eq}(T)/k_B T$. Minimizing the functional by setting $\partial\Phi/\partial\dot{a}_n=0$ for $n=-N, \ldots, N$ we obtain a system of coupled first-order ordinary differential equations for the Fourier coefficients given by

$$\sum_{m=-N}^{N} \frac{\dot{a}_m}{m} \int_0^\lambda \left(1 + \frac{|h_x|}{\epsilon}\right) e^{i(m+n)kx} \mathrm{d}x = -2in^2k^3D \int_0^\lambda \frac{\partial\gamma}{\partial h_x} e^{inkx} \mathrm{d}x. \tag{15}$$

This system of equations can be nondimensionalized by introducing the rescalings $\tilde{x}=kx$, $\tilde{a}_n=ka_n$, $\tilde{h}=kh$, $\tilde{\beta}_1=\beta_1/\beta_3$ and $\tilde{t}=D\beta_3 k^4 t$ to obtain

$$\sum_{m=-N}^{N} \frac{1}{m} \frac{\mathrm{d}\tilde{a}_m}{\mathrm{d}\tilde{t}} \int_0^{2\pi} \left(1 + \frac{|\tilde{h}_{\tilde{x}}|}{\epsilon}\right) e^{i(m+n)\tilde{x}} \mathrm{d}\tilde{x} = -2in^2 \int_0^{2\pi} \frac{\partial\gamma}{\partial\tilde{h}_{\tilde{x}}} e^{in\tilde{x}} \mathrm{d}\tilde{x}, \tag{16}$$

which can be solved by standard numerical techniques.

A key point to note here is the rescaling of real time by a relaxation rate $r(T)=D\beta_3 k^4$. If the underlying Arrhenius dependence of the microscopic parameters, $D_s(T)$, $C_{eq}(T)$ and $\kappa(T)$, is accounted for, it follows that the relaxation rate may be written as

$$r(T) = \frac{\Omega^2 \nu k^4}{k_B T} \beta_3 \mathrm{e}^{-(E_d+E_f)/k_B T} \text{ (TDL kinetics)},$$

$$= \frac{\Omega^2 h_s \nu k^4}{a k_B T} \beta_3 \mathrm{e}^{-(E_s+E_f)/k_B T} \text{ (ADL kinetics)}, \tag{17}$$

where ν is an attempt frequency, E_d is the diffusion barrier across the terrace, E_s is the barrier for adatom transport across the step edge and E_f is the adatom formation energy. Knowing the relaxation rate then allows, in principle, for the determination of the total activation energy $E=E_d+E_f$ or $E=E_s+E_f$ in the appropriate kinetic regime. For a perfectly sinusoidal modulation, the relaxation rate may be determined in a straightforward manner by monitoring the amplitude decay. The decay behavior is influenced both by the kinetics of the process and the formation energy of steps and follows the power laws summarized in Eq. (1). The situation is significantly more complicated for sputter ripples since there are several modes of comparable magnitudes present in the roughness spectrum which then leads to mode-coupling effects. Furthermore, there is no single dominant mode in the system that may be tracked since the dominance gradually shifts to lower wavelengths as the profile decays. Hence, there is no reason to believe *a priori* that the behavior of a single sinusoid may be extrapolated to a system of sputter ripples—our observations, both experimental and computational, will indeed show that the two behaviors are at variance.

IV. RELAXATION BEHAVIOR: EXPERIMENTAL AND NUMERICAL STUDIES

Having established the theoretical framework for understanding our annealing experiments and numerical studies, we now carry out detailed analyses of the same. Attention is focused first on the experimental studies and extraction of important parameters from these. Numerical simulations are discussed subsequently and are seen to be in good agreement with the experiments.

A. Experimental studies

The sputtered samples are annealed at temperatures ranging from 431 to 466 K. Figure 1(a) shows the evolution of the power spectral density (PSD) during the relaxation of one such sample annealed at 460 K. The PSDs are normalized by that of a smooth surface with negligible roughness (rms $\sim$5 Å over an area of 10 μm$\times$10 μm). At the outset, the amplitude of the profile is approximately 10 nm and the power spectrum shows the presence of several modes peaked around $k=0.0153$ nm^{-1} which roughly corresponds to a wavelength of 400 nm. The evolution of the profile is tracked over a total time of 300 min. As relaxation proceeds, the peak in the power spectrum is clearly seen to shift to longer wavelengths. The total power in the spectrum is found by integrating over the entire spectrum—the ripple amplitude $Z(t)$ is then proportional to the square root of the total power. The inset in Fig. 1(a) shows the ripple amplitude normalized by the initial amplitude plotted as a function of time. The decay behavior shows some tendency towards an inverse-linear scaling with time—one should be cautious, however, in considering this fit to be a validation of the 1D studies of Ozdemir and Zangwill (OZ)[7] and Rettori and Villain (RV).[22] In addition to considering a perfect sinusoid, both these studies only consider the effect of step interactions and ignore the line-tension contribution. The line-tension contribution is, however, critical for the formation of facets[14,15] in both the TDL and ADL regimes. AFM images of samples, shown in Fig. 2(a), taken at various stages of relaxation clearly show the presence of facets at the extrema of the profile. The RV-OZ model, in contrast, predicts a sharpening at the extrema of decaying profiles which would then suggest that the model is not applicable in the present situation. This sharpening of the profile extrema for zero line tension has also

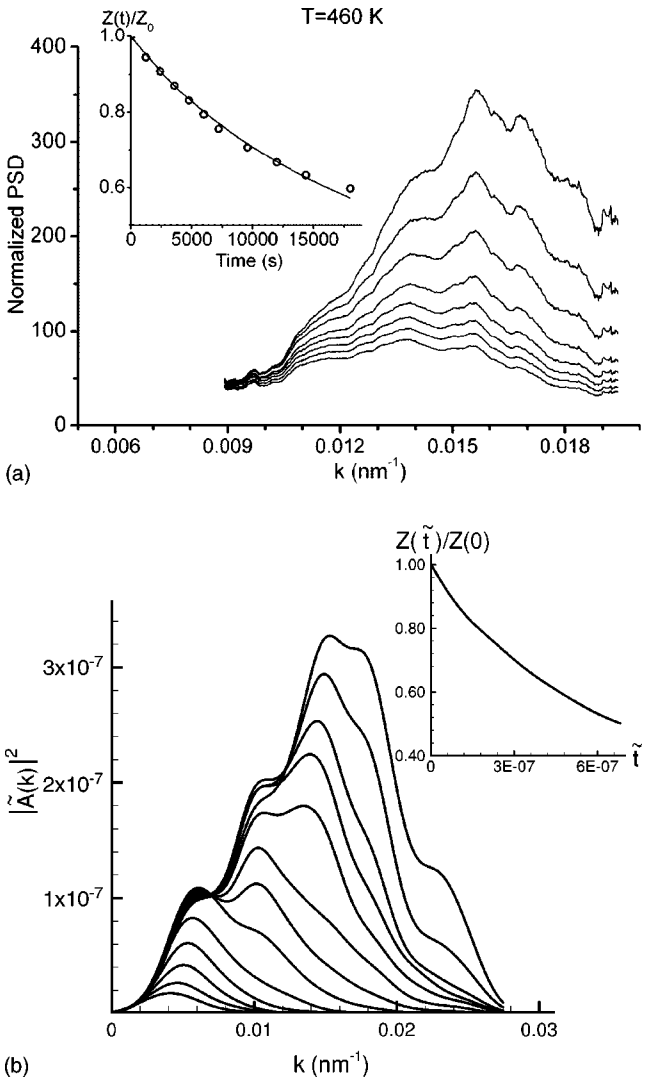

FIG. 1. Evolution of the power spectral density as the ripples relax (a) measured experimentally using LiSSP and (b) determined numerically. The surface has an initially dominant mode at $k=0.153$ and $k=0.151$ nm^{-1} in (a) and (b), respectively with a few modes of comparable magnitude around it. The short wavelength modes decay rapidly and the roughness shifts to longer wavelengths as decay proceeds. The insets in both figures show the evolution of the normalized ripple amplitude $Z(t)/Z(0)$—the decay behavior is close to inverse linear in time.

been confirmed separately in numerical studies.[14,15] Furthermore, as will be shown subsequently, the sample is expected to exhibit ADL kinetics at these temperatures. Hence, even if the inherently questionable approach of extrapolating scaling results for sinusoidal profiles to sputter ripples is adopted, the decay behavior is *not* expected to be inverse linear [see Eq. (1)].

To determine the relaxation rate $r(T)$, we monitor the decay behavior of the dominant mode $k=0.0153$ nm^{-1}. Figure 3(a) shows the decay behavior of this mode for annealing experiments at five different temperatures. By rescaling the relaxation time, these curves can be made to collapse onto each other as shown in Fig. 3(b). The relaxation rate for each anneal is then known up to a constant multiplicative factor. The relaxation rate associated with each curve may now be plotted as a function of $1/k_BT$ as shown in Fig. 4. To determine the activation energy from this curve, we still need to account for the temperature dependence of the step-interaction energy $\beta_3(T)$ as well as the prefactor in Eq. (17). Owing to the weak temperature dependence of $\beta_3(T)$ as compared to the exponential term, it is not possible to determine the additional two parameters A and ϵ_k accurately from the data—in order to proceed we use published values for these. Giesen and Einstein[23] found A for a close packed step on Cu(001) to be 7.1 ± 0.5 meV Å by analyzing the terrace width distribution using scanning tunneling microscopy (STM) imaging. The kink energy, ϵ_k, is obtained from the experiments of Giesen, Steimer, and Ibach[24] to be 0.129 eV. Using these values, we fit the data in Fig. 4 by a least-squares fit and determine the activation energy E to be 1.18 ± 0.14 eV. The measured activation energy also allows us to determine the kinetic regime of relaxation. Experimental measurements of the migration energy of adatoms E_d range from 0.36 to 0.4 eV.[25–28] The adatom formation energy E_f is approximately 0.507 eV from effective medium theory (EMT) calculation.[29] The step-edge barrier E_s, obtained from embedded atom calculations[30] and EMT calculations,[31] ranges from 0.5 to 0.7 eV and is sensitive to the actual jumping mechanism and the potential used in the simulation. From these values, the activation energy is approximately 0.8–0.9 eV for TDL kinetics and 1.0–1.2 eV for ADL kinetics. Our relaxation experiments are thus in the latter regime. Further confirmation may be obtained by estimating the parameter $2D_s|\nabla h|/\kappa h_s$ which discriminates between the two kinetic regimes. Using $1/k_BT=26$ eV^{-1}, $E_d=0.4$ eV, $E_s=0.6$ eV and an initial average slope $\langle|\nabla h|\rangle=0.05$, we obtain $2D_s|\nabla h|/\kappa h_s\approx10$ which is also indicative of ADL kinetics.

Another suggested method of establishing the kinetics of relaxation is by studying the decay of individual modes and establishing a single "universal curve" onto which these modes can be collapsed.[11] The evolution of each mode may then be described by the scaling hypothesis $A_\lambda(t)=A_\lambda(0)f(\lambda^{-m}t)$ where the exponent m, which is to be determined from the rescaling, depends upon the kinetics of the process. An important point that is often overlooked in this context is the dependence of the relaxation time on the *initial amplitude* of the mode in addition to the wavelength. Specifically, we can show that there exists a characteristic time τ for the relaxation of a sinusoid which, for various combinations of line-tension and kinetic regime, depends upon λ and $A_\lambda(0)$ as

$$\tau\sim A_\lambda(0)^{-1}\lambda^5\ (\beta_1=0),$$

$$\tau\sim A_\lambda(0)\lambda^3\ (\beta_1\neq0),\ \text{TDL kinetics},$$

$$\tau\sim\lambda^4\ (\beta_1=0),\ \tau\sim A_\lambda(0)^2\lambda^2\ (\beta_1\neq0),\ \text{ADL kinetics}. \tag{18}$$

To compare correctly the relaxation of modes that differ in wavelength as well as initial amplitude, we must then rescale the relaxation time taking into account both of these factors.

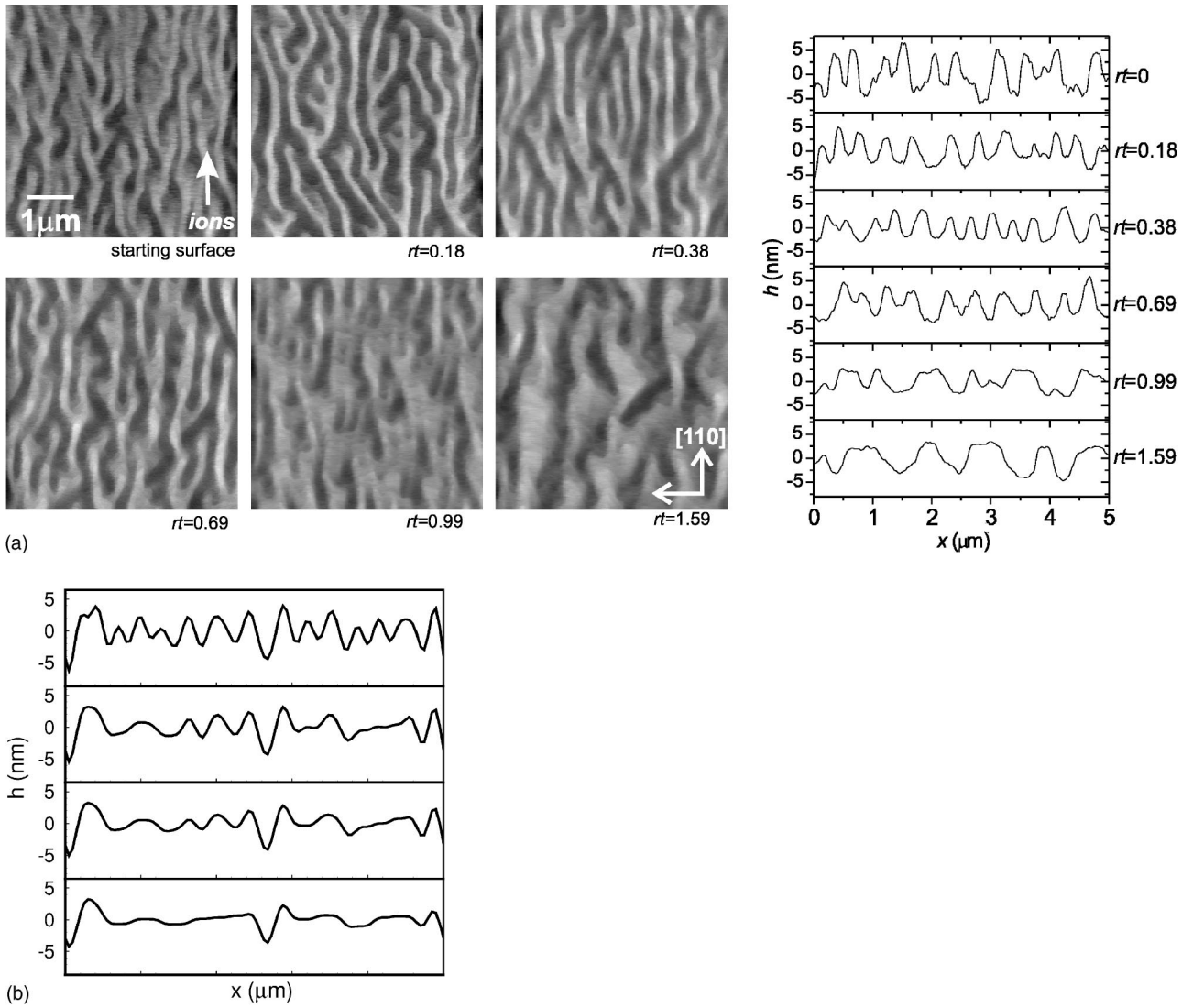

FIG. 2. (a) AFM scans of the sample at various stages of relaxation at the indicated values of rescaled time $r(T)t$. The line scans on the right are cross sections corresponding to the 2D images. Formation of facets at the peaks and valleys, as the profile decays, is clearly visible. (b) Simulated evolution of a 1D profile. The profile is reconstructed from the 2D Fourier transform of the AFM image which ensures that it is truly representative. Faceting is once again clearly visible at the peaks and valleys of the profile. The facets are seen to progressively increase in size as the profile decays. The four profiles in (b) are taken at comparable times to the first four profiles in (a), i.e., when the dominant mode in the system is 100%, 85%, 70% and 60% of its initial value. Faceting is more pronounced for the simulated profiles but the overall amplitude is approximately the same.

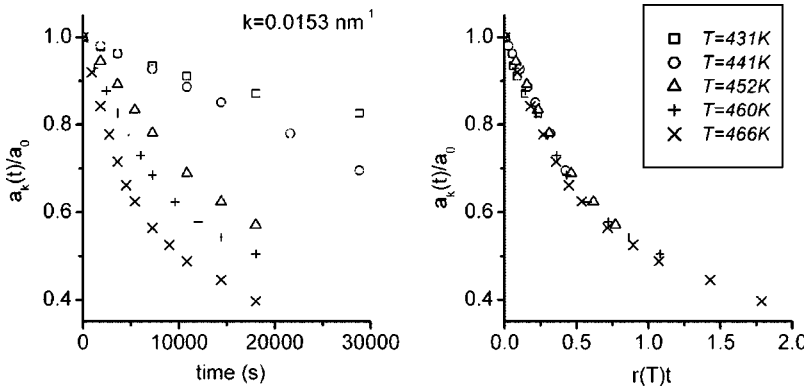

FIG. 3. (a) Evolution of the amplitude of the dominant mode $k=0.0153\ \mathrm{nm}^{-1}$ at annealing temperatures ranging from 431 to 466 K. The relaxation is faster at higher temperatures as is to be expected. The individual curves can all be collapsed onto each other, as shown in (b), by rescaling the relaxation time by a temperature dependent relaxation rate $r(T)$.

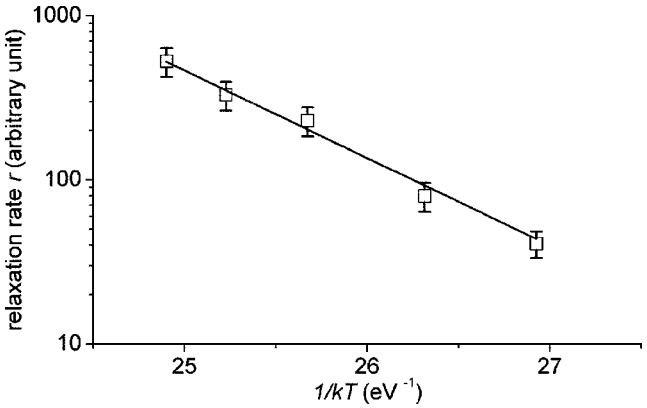

FIG. 4. Semilog plot of relaxation rate $r(T)$ for each anneal as a function of $1/k_BT$. The solid line is the least-squares fit to Eq. (17). The slope of this line gives the activation energy to be 1.18 ± 0.14 eV.

If these results for a single sinusoid are assumed to hold in general, we expect data collapse to occur when the relaxation time for each mode is rescaled as $A_\lambda(0)^{-2}\lambda^{-2}t$ for the present combination of nonzero line tension and ADL kinetics. Figure 5(a) shows the decay of the initially dominant modes in the system peaked about $k=0.0153$ nm^{-1}. Some of the modes may be collapsed onto each other by rescaling the relaxation time as k^4t [Fig. 5(b)]. This data collapse is, however, by no means ubiquitous. Modes that are further away from the peak show marked deviations from this behavior with some of the lower wavelength modes even showing an *increase* initially. The nonlinearity and mode coupling inherent in the problem thus precludes any simple scaling prediction based on the decay of a single sinusoid.

B. Numerical studies

The numerical method outlined in Sec. III is now used to simulate a representative sputter ripple sample. Since the numerical method is Fourier based, the roughness spectrum can be used directly to generate the computational sample. As mentioned previously, we use a 1D profile in our calculations, but this is in no way an inherent limitation of the calculations—the extension to a 2D profile is straightforward and the results are essentially identical owing to the elongated nature of the ripples. The parameters used in the calculation are $\beta_1=43$ meV/Å^2 (Ref. 32), $\beta_3=6$ meV/Å^2 and $\epsilon\equiv(2D_s/\kappa h_s)^{-1}=0.005$ which may be computed from the activation energies given in the previous section. By examining the initial roughness spectrum of the sample, we find that the ansatz for the surface shape may be truncated at $N=20$ which captures in sufficient detail the peak at $k=0.015$ nm^{-1} and the surrounding modes. Starting from this initial shape, the ordinary differential equations for the Fourier coefficients are integrated using a standard Runge-Kutta routine. Figure 1(b) shows the PSD during various stages of the evolution. The initial peak at $k=0.0151$ nm^{-1} is seen to gradually decay with longer wavelength modes becoming dominant over time—there is even a tendency for some of the longer wavelengths to show a slight increase at first as seen around $k=0.006$ nm^{-1}. The inset shows the evolution of the ripple amplitude $Z(t)=\sqrt{\Sigma_{n=-N}^{N}|a_n(\tilde{t})|^2}$ normalized by the initial amplitude $Z(0)$—the decay is nearly inverse linear in agreement with the experimental results but, as mentioned previously, is not anticipated from studies of the decay of a single sinusoid in the ADL regime. The surface profile at various stages of decay is shown in Fig. 2(b). Faceting is clearly seen at the extrema owing to the line-tension contri-

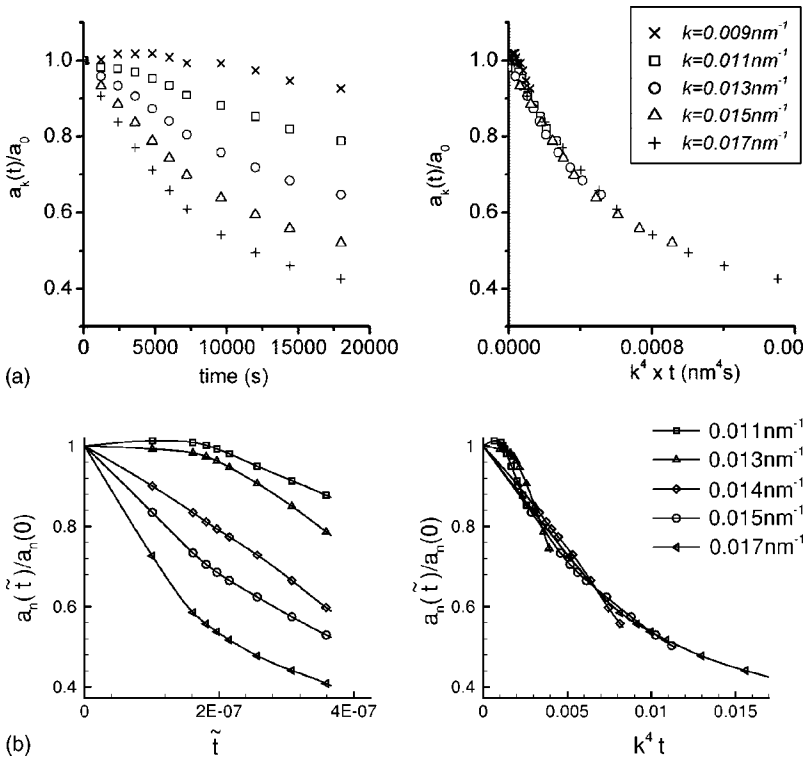

FIG. 5. (a) Experimentally measured decay of the normalized amplitudes of a few modes around the initial peak at $k=0.153$ nm. The relaxation time may be rescaled as k^4t for each wave number k and the curves re-plotted as in (b). There is some evidence for data collapse over a short time. (c) Numerical calculations for the decay of modes present around the initial peak in the spectrum at $k=0.151$ nm and (d) the same decay curves with time rescaled as k^4t. A few of the modes show data collapse over 40%–50% amplitude decay, but some modes clearly show deviations owing to their tendency to increase initially.

bution (nonzero step-formation energy). Short wavelength features disappear rapidly and longer wavelengths are seen to dominate as decay proceeds. The numerical results, thus far, are qualitatively in good agreement with the experiments.

To verify the wavelength scaling hypothesis introduced previously, we track the temporal evolution of each mode and look for possible data collapse by rescaling the decay time for each mode. Figure 5(c) shows the decay of the initially dominant modes in the roughness spectrum plotted as a function of nondimensionalized time while Fig. 5(d) shows the same curves plotted for $m=4$, i.e., for a rescaling of relaxation time as k^4t. A few modes are found to collapse onto each other to a reasonable degree (around 40%–50% amplitude decrease) but some of the longer wavelength modes do not conform to this scaling owing to a tendency to *increase* initially. Additionally, there are several other modes in the spectrum (which have not been shown in the figure to maintain clarity) that show no data collapse whatsoever. It is worth recalling here the expected behavior for a single sinusoid on the basis of which such scaling hypotheses are made. The amplitude decay of a perfect sinusoid in the ADL regime with nonzero line-tension contribution is shown in Fig. 6(a). The decay behavior is seen to follow the scaling $a(\tilde{t}) \sim a_0\sqrt{\tilde{t}^*-\tilde{t}}$ from which it follows that $a(t)\sim a_0\lambda^{-2}\sqrt{t^*-t}$. This scaling prediction has been confirmed independently by kinetic Monte Carlo simulations.[15] If this result is now extrapolated to the sputter-ripple case, a wavelength scaling with $m=4$ is not anticipated. We are thus led to conclude that simple scaling hypotheses, based on the study of ideal sinusoids, are unlikely to be applicable to more complicated nonlinear systems with pronounced mode-coupling effects.

While our numerical calculations are in good agreement qualitatively with experiments, it is useful to estimate activation energies to make a quantitative connection. Specifically, assuming E_d and E_f to be known inputs to the model, E_s should be readily available from the relaxation data. By comparing relaxation times from the experimental and simulated curves for $Z(t)/Z(0)$ and using the relaxation rate for ADL kinetics given in Eq. (17), the total activation energy is found to be approximately 0.95 eV which implies that $E_s \approx 0.45$ eV. This is slightly lower than the values of 0.5–0.7 eV cited previously, but nevertheless indicates that a simple continuum model with few parameters can indeed capture both qualitatively and quantitatively, several features of the actual experiment.

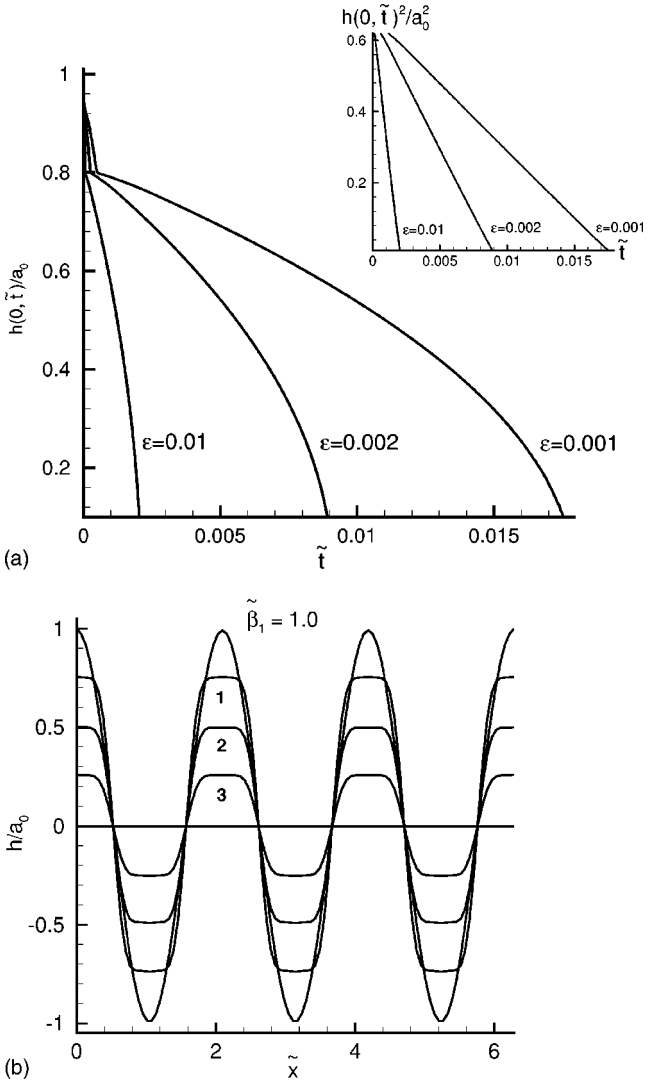

FIG. 6. (a) Normalized amplitude $h(0,\tilde{t})/a_0$ plotted as a function of rescaled time $\tilde{t}$ for the decay of a 1D sinusoid for different values of ϵ with $\tilde{\beta}_1=1.0$. The initial condition is $h(x,0)=0.033\cos(3kx)$. As ϵ decreases, the kinetics is increasingly dominated by attachment and detachment of atoms at a step edge. The inset shows the same curves with the vertical axis now being $h^2(0,\tilde{t})/a_0^2$ and the initial transient suppressed. For small values of ϵ, the curves are linear thus indicating that $h(0,\tilde{t})\sim\sqrt{\tilde{t}^*-\tilde{t}}$ in the attachment-detachment regime, $\tilde{t}^*$ being the time at which the amplitude vanishes. The decay profiles shown in (b) clearly indicate the formation of facets at the extrema owing to nonzero line tension. The profiles denoted by 1, 2 and 3 are self-similar, the size of the facets remaining constant during this stage of decay.

V. CONCLUDING REMARKS

In summary, we have studied the relaxation behavior of nano-ripples on Cu(001) by experimental and numerical techniques. The underlying physics of crystallographic steps is used to provide a theoretical framework within which the results can be understood. Statistically similar samples are annealed over a temperature range and the relaxation monitored by LiSSp and AFM imaging. This allows us to monitor the overall amplitude evolution as well as the evolution of individual modes in the roughness spectrum. Numerical studies are conducted on a representative sputter-ripple profile with realistic parameters. The observations from experiments and numerics are found to be in good agreement, both qualitatively and quantitatively. Our experiments are in the ADL regime with a perceptible line-tension contribution visible from the faceting at the profile extrema. We incorporate these features into our numerical method, unlike previous studies, and obtain the necessary parameters from published atomistic and STM studies. The total activation energy for the relaxation process is measured to be 1.18 ± 0.14 eV experimentally and 0.95 eV numerically. Our continuum model is thus able to reproduce the actual situation to a good degree

with only a few parameters for inputs. We find some propensity for inverse-linear scaling of amplitude decay with time, but this analytical form does not come out obviously from the theory. The similarity of this decay with earlier predictions based on single sinusoid decay is likely fortuitous. We also find a tendency for a few modes, situated around the initial peak in the spectrum, to show data collapse under a rescaling of time by λ^{-4}, although we do not have sufficiently extensive measurements to rule out other possible scalings. There are, however, several other modes in the spectrum which do not conform to such a scaling with some of the longer wavelengths even showing an increase over appreciable times. We conclude that scaling observations based on the behavior of perfect sinusoids are unlikely to hold for the present case which is more complicated owing to the nonlinearity of the problem and mode-coupling effects.

Our modeling approach here has been kept simple with line tension, surface diffusion barriers and step-edge barriers assumed to be isotropic. The inclusion of anisotropy is, in principle, straightforward and will be investigated in the future. The relaxation behavior is likely to be influenced by the crystallographic orientation of the sputtered surface as well as the orientation of ripples along the surface—further experiments are proposed to address these issues. It is also possible to take the experiments further into the ADL regime with lower annealing temperatures and is an issue of current investigation.

ACKNOWLEDGMENTS

W.L.C. and E.C. are pleased to acknowledge support from the U.S. Department of Energy under Contract No. DE-FG02-01ER45913. A.R. and V.B.S. gratefully acknowledge the research support of the National Science Foundation through Grant Nos. CMS-0093714 and CMS-0210095 and the Brown University MRSEC program through Grant No. DMR-0079964.

*Electronic address: Vivek_Shenoy@brown.edu

[1] C. Herring, *Structure and Properties of Solid Surfaces*, edited by R. Gomer and C. S. Smith (University of Chicago Press, Chicago, 1953), p. 5.
[2] W. W. Mullins, J. Appl. Phys. **28**, 333 (1957).
[3] J. M. Blakely and H. Mykura, Acta Metall. **10**, 565 (1962).
[4] P. S. Maiya and J. M. Blakely, J. Appl. Phys. **38**, 698 (1967).
[5] H. P. Bonzel, E. Preuss, and B. Steffen, Appl. Phys. A: Solids Surf. **35**, 1 (1984).
[6] H. Spohn, J. Phys. I **3**, 69 (1993).
[7] M. Ozdemir and A. Zangwill, Phys. Rev. B **42**, 5013 (1990).
[8] N. Israeli and D. Kandel, Phys. Rev. B **62**, 13 707 (2000).
[9] J. Erlebacher and M. J. Aziz, Surf. Sci. **374**, 427 (1997).
[10] M. V. Ramana Murty, Phys. Rev. B **62**, 17 004 (2000).
[11] J. Erlebacher, M. J. Aziz, E. Chason, M. B. Sinclair, and J. A. Floro, Phys. Rev. Lett. **84**, 5800 (2000).
[12] L. Pedemonte, G. Bracco, C. Boragno, F. Buatier de Mongeot, and U. Valbusa, Phys. Rev. B **68**, 115431 (2003).
[13] J. Blakely, C. Umbach, and S. Tanaka, *Dynamics of Crystal surfaces and interfaces*, edited by P. M. Duxbury and T. J. Pence (Plenum, New York, 1997), p. 23.
[14] V. B. Shenoy, A. Ramasubramaniam, and L. B. Freund, Surf. Sci. **529**, 365 (2003).
[15] V. B. Shenoy, A. Ramasubramaniam, H. Ramanarayan, D. T. Tambe, W. L. Chan, and E. Chason, Phys. Rev. Lett. **92**, 256101 (2004).
[16] W. L. Chan, N. Pavenayotin, and E. Chason (to appear in Phys. Rev. B).
[17] E. Chason, M. B. Sinclair, J. A. Floro, A. Hunter, and R. Q. Hwang, Appl. Phys. Lett. **72**, 3276 (1998).
[18] H.-C. Jeong and E. D. Williams, Surf. Sci. Rep. **34**, 177 (1999).
[19] G. Ehrlich and F. G. Hudda, J. Chem. Phys. **44**, 1039 (1966).
[20] R. L. Schwoebel, J. Appl. Phys. **40**, 614 (1969).
[21] P. Noziéres, J. Phys. (France) **48**, 1605 (1987).
[22] A. Rettori and J. Villain, J. Phys. (France) **49**, 257 (1988).
[23] M. Giesen and T. L. Einstein, Surf. Sci. **449**, 191 (2000).
[24] M. Giesen, C. Steimer, and H. Ibach, Surf. Sci. **471**, 80 (2001).
[25] M. Breeman and D. O. Boerma, Surf. Sci. **269,270**, 224 (1992).
[26] H. Durr, J. F. Wendelken, and J. K. Zuo, Surf. Sci. **328**, L527 (1995).
[27] M. C. Bartelt, L. S. Perkins, and J. W. Evans, Surf. Sci. **344**, L1193 (1995).
[28] J. J. De Miguel, A. Sanchez, A. Cebollada, J. M. Gallego, J. Ferron, and S. Ferrer, Surf. Sci. **189-190**, 1062 (1987).
[29] P. Stoltze, J. Phys.: Condens. Matter **6**, 9495 (1994).
[30] M. Karimi, T. Tomkowski, G. Vidali, and O. Biham, Phys. Rev. B **52**, 5364 (1995).
[31] J. Merikoski, I. Vattulainen, J. Heinonen, and T. Ald-Nisilla, Surf. Sci. **387**, 167 (1997).
[32] F. Raouafi, M. C. Desjonqueres, and D. Spanjaard, Surf. Sci. **505**, 183 (2002).
[33] In a previous publication, Shenoy *et al.* (see Ref. 14) have shown that the decay of a 2D sinusoid smoothly approaches the behavior of a 1D sinusoid as one of the wavelengths of the modulation diverges. For the present work, we have also carried out 2D calculations for sputter-ripple systems and found the behavior to be nearly identical to that predicted by the much less computationally intensive 1D analog.